Supporting Information

High speed electrically switching reflective structural color display with large color gamut

Wenqiang Wang[1], Zhiqiang Guan[1,*], Hongxing Xu[1,2,*]

1 School of Physics and Technology, Center for Nanoscience and Nanotechnology, and Key Laboratory of Artificial Micro- and Nano-structures of Ministry of Education, Wuhan University, Wuhan 430072, China
2 The Institute for Advanced Studies, Wuhan University, Wuhan 430072, China

Authors' email addresses:
Hongxing Xu: hxxu@whu.edu.cn. Phone: +8627 6875 2253.
Zhiqiang Guan: zhiqiang.guan@whu.edu.cn. Phone: +86186 2715 4793.

1 Mesh grids setting and convergence test in FDTD simulations

Non-uniform mesh settings were used in the FDTD simulations. An overriding mesh with minimum grid size dx = dy =1.2 nm was added in the grating, ITO and Al_2O_3 film region. The minimum grid size of 1.2 nm was determined by the convergence test in Fig. S1.

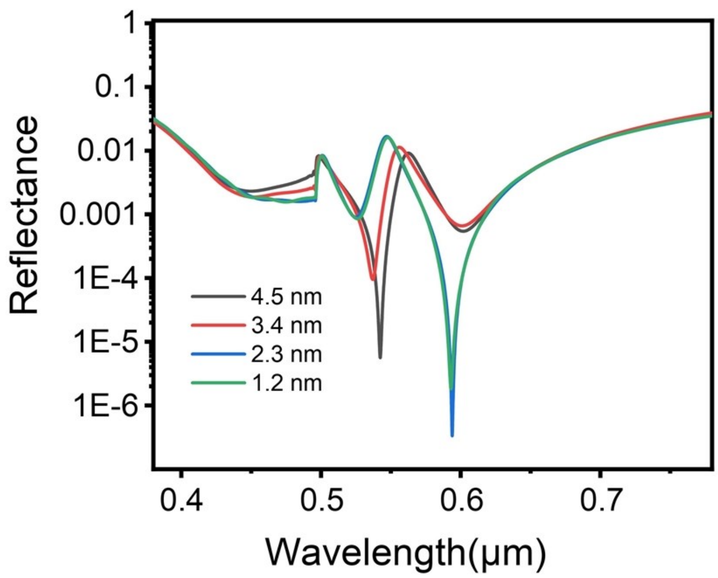

Fig. S1. The reflectance spectra for Green pixel at color-off state with different minimum grid size.

2 The influence of ITO_{active} layer thicknesses on the anti-reflection at color-off state

Different ITO_{active} layer thicknesses were used at different wavelength range in the references, like 5±1 nm at 0.5 μm ~ 0.8 μm,[1] 1.5 nm at ~ 4 μm,[2] 0.9 nm at 1.55 μm.[3] We evaluated the influence of ITO_{active} layer thicknesses on the anti-reflection at the green pixel's color-off state through RCWA method in Fig. S2. T_{acc} = 0.5 nm was thick enough to suppress reflectance below 3.5% and guaranteed a good anti-reflection effect. Larger T_{acc} values gave wider carrier-concentration work windows with sufficient low reflectance. And in visible region, T_{acc} can be 5 nm according to reference.[1] So the compromised T_{acc} value of 2.5 nm could ensure the satisfied modulation effect with reduced practical control requirement and was used in the main text.

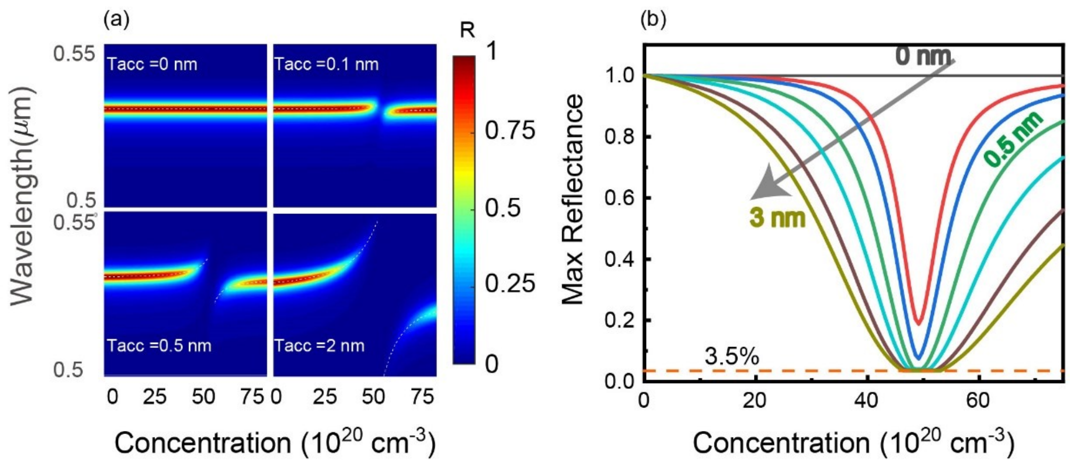

Fig. S2 (a) The reflectance spectra vs. carrier concentration contour plot for different

T_{acc}. (b) The maximum reflectance vs. electron concentration for different T_{acc}.

3 Extraction of the effective index n_{eff}

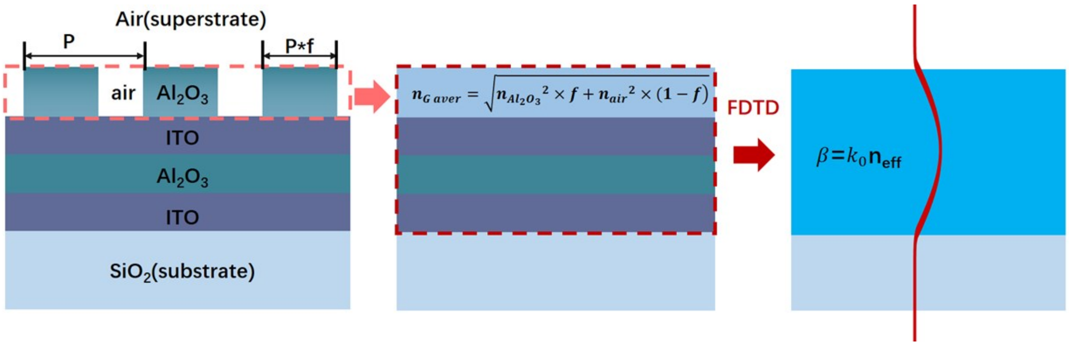

Fig. S3 Extraction of the effective index n_{eff}.

The GMR grating has a sub-wavelength period. Thus the 0 order diffraction is the main channel.[4] We extracted the effective index of the GMR grating as below. The Al_2O_3 grating layer was treated as a homogeneous film with a refractive index $n_{G\_aver} = \sqrt{n_{Al_2O_3}{}^2 \times f + n_{air}{}^2 \times (1-f)}$. The effective refractive index of the GMR grating equals to that of the n_{G_aver}/ITO/Al_2O_3/ITO four-layer system and was calculated by FDTD method.

4 Reflectance, transmittance and absorptance spectra of the green pixel at color-on/off state.

The reflectance near the resonance wavelength changed at least two orders and the transmittance changed about five orders between color-on and color-off state.

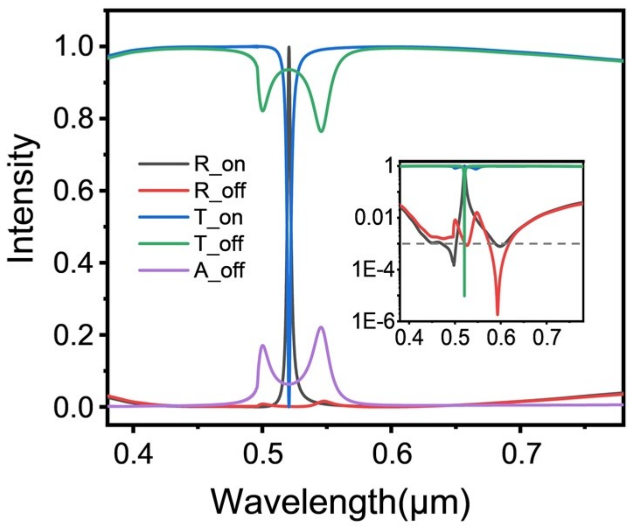

Fig. S4 The Reflectance, transmittance and absorptance spectra for the green pixel at color-on/off state. The inset shows the transmittance and reflectance spectra in the logarithmic scale. The structure parameters are in Table 1 in the main text.

5 The GMR grating response under TE polarized light

The reflectance spectra of the GMR grating at the color-on/off state under TE polarization were plotted in Fig. S5(a). The modulation effect was much weaker than that under TM polarization. At color-on state, the reflection peak is at 541 nm, and at color-off state, the reflection peak moves to 539 nm. The reflection peak position is explained by the effective mode index theory.[4] The reflection peaks were predicted by the intersections between the effective index of the films $n_{eff_on}$and n_{eff_GV}. The weak modulation effect was explained in the main text from the electric field distribution analysis. The vertical electric field component is almost zero. So the ENZ material-induced funneling effect was weak, and the reflectance was less affected. The slightly reduced reflection at color-off state was due to the increased optical loss in the ITO_{active} layer as it changed from lossless material to lossy material.

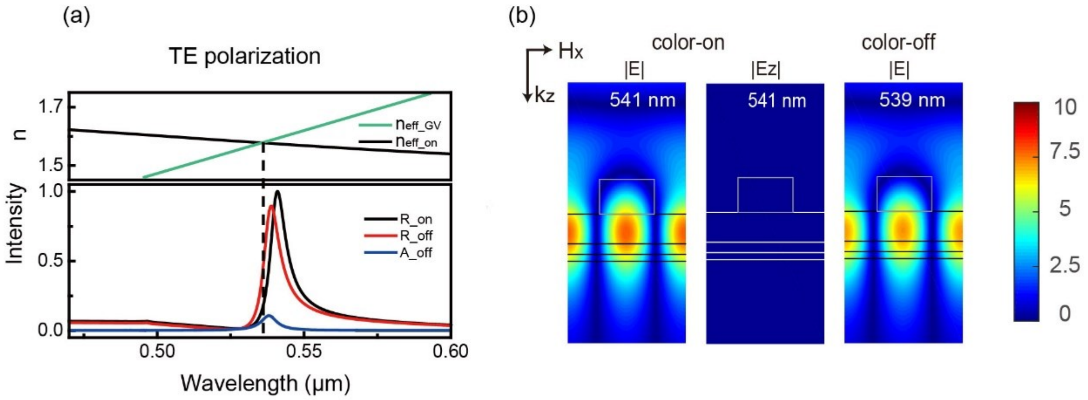

Fig. S5 (a) Up panel: The wavelength-dependent effective refractive index of the grating vector n_{eff_GV} (green line) and the GMR grating n_{eff_on} (black line). n_{eff_off} was not shown as it was almost the same as n_{eff_on}. Bottom panel: the reflectance spectrum at color-on state (black line), the reflectance and absorptance spectra at color-off state (red and blue line). (b) The electric field distributions of |E| or $|E_z|$ in the cross-section of the GMR grating at the reflectance peak wavelength at color-on or color-off state.

6 The incident angle-dependent reflectance spectra under TM polarization.

The reflectance spectra are sensitive to the incident angle.

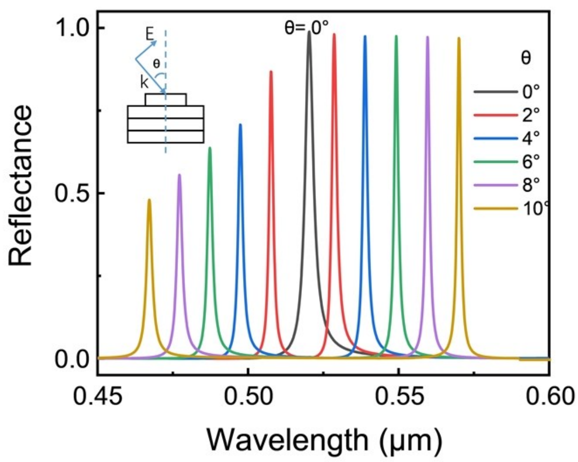

Fig. S6 The reflectance spectra for different incident angles under TM polarization for the green pixel. The structure parameters are in Table 1 in the main text.

7 The reflectance spectra of the red and blue pixel with different grating period numbers at color-on state

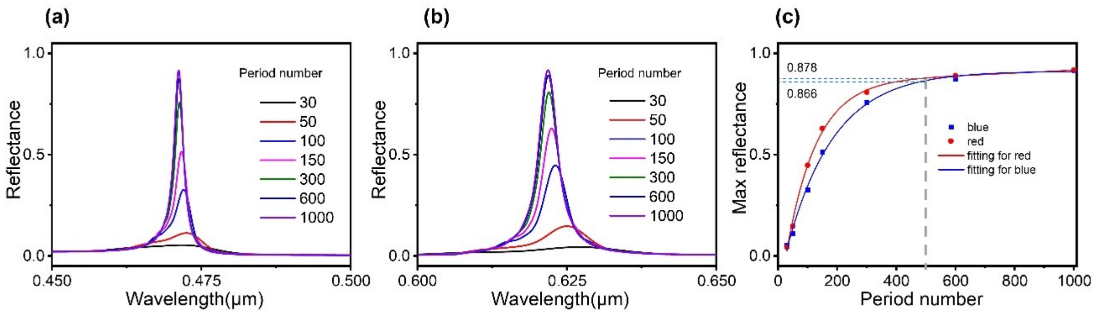

Fig. S7 The reflectance spectra with different period numbers for blue (a) or red (b) pixel. (c) The maximum reflectance dependence on the grating period numbers for blue or red pixels. The structure parameters are in Table 1 in the main text.

The display performances for red, green, and blue pixels with fixed grating period number $N_p = 500$ are summarized as Table S1. The structure parameters are in Table 1 in the main text.

Table S1 The display performances for red, green, and blue pixels with fixed grating period $N_p = 500$.

	Peak intensity	Operation speed (MHz)	DPI
Red	87.8%	13.4	86
Green	90%	20.1	105
Blue	86.6%	25.6	119

8 Realization of RGB primary colors by purely changing GMR grating period

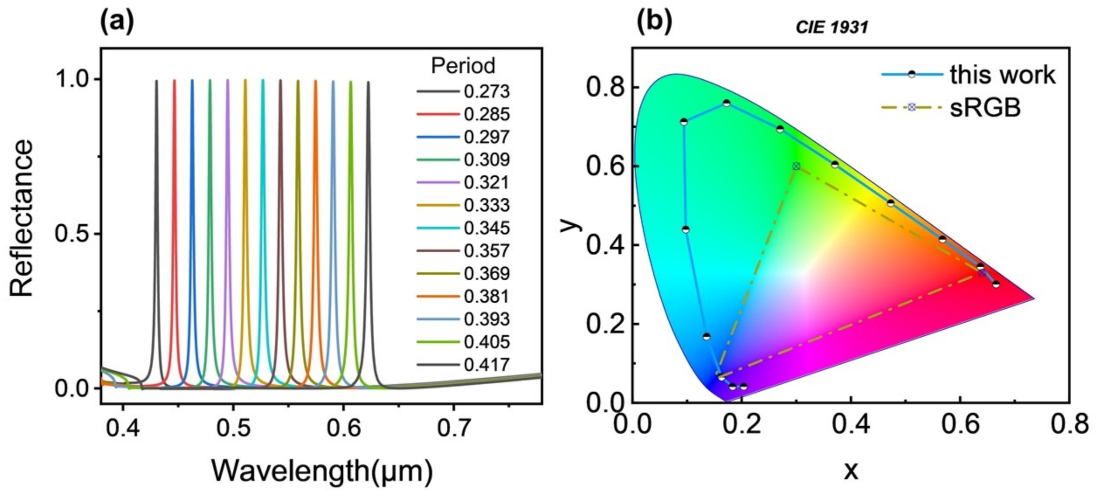

Fig. S8. (a) The reflectance spectra for different grating periods. (b) The corresponding color gamut in CIE 1931 coordinates. The other geometric parameters are taken from the green pixel in Table 1 in the main text.

Table S2. The display performance of the green pixel with different period numbers.

N_p (Period number)	Peak intensity	Color gamut [in unit of sRGB area]	operation speed [MHz]	DPI
30	9.16%	77%	3712	1435
50	23.7%	113%	1336	861
90	50%	133%	412	478
100	56.4%	140%	334	430
113	60%	142%	262	381
150	71%	148%	148	287
300	84.4%	155%	37.1	143
500	90%	157%	13.4	86
600	91.7%	158%	9.28	71
1000	94.6%	159%	3.34	43
∞	99.7%	161%	--	--

References

1. E. Feigenbaum, K. Diest and H. A. Atwater. Unity-order index change in transparent conducting oxides at visible frequencies, *Nano Lett*, 2010, **10**, 2111-2116.
2. J. Park, J. H. Kang, X. Liu and M. L. Brongersma. Electrically Tunable Epsilon-Near-Zero (ENZ) Metafilm Absorbers, *Sci. Rep.*, 2015, **5**, 15754.
3. Y.-W. Huang, H. W. H. Lee, R. Sokhoyan, R. A. Pala, K. Thyagarajan, S. Han, D. P. Tsai and H. A. Atwater. Gate-Tunable Conducting Oxide Metasurfaces, *Nano Lett.*, 2016, **16**, 5319-5325.
4. S. S. Wang and R. Magnusson. THEORY AND APPLICATIONS OF GUIDED-MODE RESONANCE FILTERS, *Appl. Opt.*, 1993, **32**, 2606-2613.